Ion-Channel Formation Assisted by Electrostatic Interhelical Interactions in Covalently Dimerized Amphiphilic Helical Peptides[†]

Junichi Taira,[‡] Masoud Jelokhani-Niaraki,[§] Satoshi Osada,[‡] Fumio Kato,[||] and Hiroaki Kodama*[,‡]

Department of Chemistry, Faculty of Science and Engineering, Saga University, Saga 840-8502, Japan, Department of Chemistry, Faculty of Science, Wilfrid Laurier University, Waterloo, Ontario N2L 3C5, Canada, and Department of Applied Biological Science, Faculty of Agriculture, Saga University, Saga 840-8502, Japan

Received December 4, 2007; Revised Manuscript Received January 16, 2008

ABSTRACT: An ultimate goal of synthetic ion-channel peptide design is to construct stable and functional ion-conducting pores. It is expected that specific interhelical interactions would facilitate the association of helices in phospholipid membranes and the successive helix-bundle formation. In the present study, we rationally designed helix-bundle ion channels using the synthetic hybrid peptide K20E20, a disulfide dimer of cationic- and anionic-amphiphilic helices Ac-CGG-$(BKBA)_5$-NH_2 and Ac-CGG-$(BEBA)_5$-NH_2. Circular dichroism (CD) measurements in aqueous media implied helix stabilization in the peptide caused by the interhelical electrostatic interactions. In addition, CD spectra recorded in the presence of DPPC liposomes and dye-leakage measurements suggested a high degree of association of peptide monomers in phospholipid membranes as well as high affinities between peptide and lipid bilayers. These features allowed ion-channel formation at extremely low peptide concentrations (as low as 1 nM). According to electrophysiological analyses, stable helix bundles were constructed of six peptide helices by association of three K20E20 molecules. Helix−helix association in lipid membranes, peptide−membrane interactions, and ion-channel formation of K20E20 peptides were all facilitated by intramolecular electrostatic interactions between the helices of the hybrid peptide and were pH-dependent. Conductance through K20E20 ion channels decreased under acidic conditions because of the interruption of the salt bridges.

Ion-channel peptides form ion-conducting structures in lipid membranes. These peptides possess diverse structures, such as α-helix, β-helix, 3_{10}-helix, and can be either linear or cyclic (*1*–*5*). A large number of structure–activity relationship studies have been dedicated to α-helical ion-channel peptides. The widely accepted ion-conducting mechanism for α-helical peptides is known as the "barrel-stave" model (*6*), which involves an assembly of α-helical monomers to form a bundle with a central ion-conducting pathway. Similar helix-bundle motifs are also found in the pore regions of integral membrane ion-channel proteins; therefore, the bundles of natural or synthetic α-helical ion-channel peptides have served as prototypes for ion-channel proteins because of their reduced structural complexity compared to proteins (*7*). Especially, *de novo* synthesis of model ion-channels composed of α-helical peptides has provided groundwork for the design of novel synthetic molecules with desired ion-channel properties (*8, 9*). In this approach, the construction of stable ion-conducting pores at low peptide concentrations has been considered as the primary step in developing synthetic ion-channel scaffolds. In addition, controlling the size of the helical-bundle construct is also required for favorable modifications of the channel functions, such as a regulation of ion conductance and ion selectivity.

Generally, the formation of helix bundles involves the binding of helices to lipid membranes, their successive insertion, and the formation of higher order structures by contacts between helices. Thus, investigating helix−helix interactions in phospholipid bilayers would be an appropriate approach to address these processes. The helix bundle would need to contain more than two monomeric helices if they were to provide an ion-conducting pathway, and two-stranded coils might occur as intermediates in the bundle-assembly process. DeGrado et al. reported on ion channels formed from a 21-meric amphiphilic α-helix peptide composed of Ser and Leu residues and noted that the peptide could form two-stranded or higher ordered coiled-coil-like structures (*2, 8*). Chung et al. reported that the dimeric form of the peptide is a major component of the peptide−lipid membrane equilibrium (*10*). Woolley and Wallace also suggested the spontaneous dimerization of alamethicin in lipid bilayers using circular dichroism (CD)[1] techniques (*11*). Hence, it is expected that stabilizing the two-stranded helical peptides would directly promote the formation of helix-bundle assemblies. Moreover, appropriate tertiary-structure contact of helices should facilitate pore formation with desired structures and physicochemical properties. Basically, in aqueous environments, the stable helix associations are dominantly

[†] This work was supported in part by Grants-in-Aid for Scientific Research (C) (18550154) and for JSPS Fellows (17-6431) from the Ministry of Education, Culture, Sports, Science, and Technology of Japan. J.T. is grateful for the JSPS Research Fellowship for Young Scientists.

* To whom correspondence should be addressed: Department of Chemistry, Faculty of Science and Engineering, Saga University, 1 Honjo, Saga 840-8502, Japan. Telephone: +81-952-28-8562. Fax: +81-952-28-8548. E-mail: hiroaki@cc.saga-u.ac.jp.

[‡] Faculty of Science and Engineering, Saga University.

[§] Wilfrid Laurier University.

[||] Faculty of Agriculture, Saga University.

10.1021/bi702371e CCC: $40.75
Published on Web 02/27/2008

induced by hydrophobic interactions, such as the coiled-coil model peptides developed by Hodges and co-workers (*12–15*). On the other hand, a great majority of designed α-helical ion-channel peptides are amphiphilic with a distribution of hydrophilic and hydrophobic surfaces on opposite sides of the helix (*2, 8*). In the helical bundles composed of amphiphilic helices, the hydrophobic interaction occurs between hydrophobic surfaces of helices and the hydrophobic core of phospholipid bilayers. Therefore, enhancement of helix−helix interactions via hydrophobic surfaces is not appropriate for peptide association in hydrophobic environments. Recently, interactions between the side chains of polar residues have been used for the promotion of helix association in lipid bilayers or detergent micelles [e.g., hydrogen-bond (*16–19*) and cation−π interactions (*20*)]. These interactions have been incorporated into coiled-coil peptides (*16*), protein transmembrane helical segments (*17*), as well as polyleucine (*18*) and helix–loop–helix peptide analogues (*19*). Consequently, in recent years, substantial information has been accumulated on the appropriate arrangements of amino acids to promote helical peptide associations.

In the present study, ion pairs were incorporated into synthetic ion-channel molecules to facilitate helix-bundle formation. A series of homo- and heterodimeric cationic and/or anionic helical ion-channel peptides were designed and synthesized. When ion pairs are formed between hydrophilic surfaces of the cationic and anionic helices in the heterodimeric peptides, enhancement of helix association and subsequent channel formation in the phospholipid bilayers are expected without the interference of the peptide−bilayer hydrophobic interactions. In addition, degradation of the electrostatic interhelical interactions caused by peptide dilution could be avoided by covalent peptide dimerization. Monomeric cationic and anionic peptide sequences employed in the present study have been developed in our laboratory as templates for synthetic channel-forming peptides (*21–23*). In comparison to more complex sequences of natural ion-channel peptides or transmembrane segments derived from natural ion-channel proteins, our helical ion-channel peptides provide a simple and straightforward model for studying effects of the electrostatic interactions on ion-channel properties.

An alternative purpose of this study is the application of the electrostatic interaction for the regulation of channel function. One of the goals in the design of model synthetic peptide ion–channel constructs is to transmit signals from external stimuli as ionic currents across the membrane through peptide ion–channels. Futaki et al. used specific molecular recognition of the host–guest chemistry [e.g., protein metal-binding domain versus metal ion (*24*), biotin–avidin interaction (*25*)] for ion-channel activation. These approaches are classified as ligand-gating models of ion channels. In the present study, because ion-channel formation has been facilitated through intramolecular salt-bridge formation, the channel-forming ability would be influenced by pH conditions. The influence of pH on the conformation and ion-channel properties of the chimeric helices is therefore studied to examine the effect of disruption of the intramolecular electrostatic interactions on ion-transport activities.

EXPERIMENTAL PROCEDURES

Materials. *N*-α-Fmoc-protected amino acids, 2-(1*H*-benzotriazole-1-yl)-1,1,3,3-tetramethyl-uronium hexafluorophosphate (HBTU), and 4-(2′,4′-dimethoxyphenyl-Fmoc-aminomethyl)phenoxy resin (Rink amide resin) were purchased from Novabiochem (Tokyo, Japan). *N*,*N*-dicyclohexylcalbodiimide (DCC), 1-hydroxybenzotriazole (HOBt), and 2,2,2-trifluoroacetic acid (TFA) were available from the Peptide Institute (Osaka, Japan). Diphytanoylphosphatidylcholine (DPhPC) was obtained from Avanti Polar Lipids (Alabaster, AL) as 50 mg/mL chloroform solutions. Dipalmitoylphosphatidylcholine (DPPC) was purchased from Sigma (Tokyo, Japan). All other chemicals were obtained from Wako Pure Chemical Industries (Osaka, Japan) and used as received.

Peptide Synthesis. The peptide elongations were carried out by 9-fluorenylmethoxycarbonyl (Fmoc) solid-phase peptide synthesis on Rink amide resin (0.61 mmol/g, 50 mmol scale as 1 equiv). A total of 10 equiv of *N*-α-Fmoc-protected amino acids were preactivated with HBTU−HOBt in the presence of *N*,*N*-diisopropyl-ethylamine (DIEA) for 20 min. Then, the coupling reaction was carried out for 40 min at room temperature. Fmoc groups were removed by 20% piperidine/*N*,*N*-dimethylformamide (DMF) treatments for 10 min. After the peptide elongation, N termini were acetylated for 3h by preactivation of AcOH with DCC/HOBt. Crude linear products were cleaved from the resins by TFA treatments containing 5% triisopropylsilane (TIS) and 5% H_2O for 90 min. The filtrates were concentrated under N_2 breezing, and then crude products were obtained from ether precipitation. The crude linear peptides were purified by reversed-phase high-performance liquid chromatography (RP-HPLC) on a Wakosil 5C4–200 column (φ 10.0 × 250 mm). Peptide dimerizations via disulfide bond formation were performed by air oxidation of termini Cys side chains. Monomeric peptides were dissolved in aqueous solution and then bubbled for 12–24 h. The progress of the air oxidation was monitored by analytical RP-HPLC on a Wakosil 5C4–200 column (φ 4.0 × 150 mm). After air oxidation, dimeric peptides were repurified by the semipreparative RP-HPLC. The purities of the peptides were confirmed by the analytical RP-HPLC. The structures of peptides were verified by matrix-assisted laser desorption ionization time-of-flight mass spectrometry (MALDI−TOF MS) analyses. MALDI−TOF MS for K20K20, E20E20, K20E20, and anti-K20E20 was 4245.1 [expected for $(M + H)^+$, 4243.6], 4276.2 [expected for $(M + Na)^+$, 4275.0], 4249.7 [expected for $(M + H)^+$, 4248.3], and 4249.4 [expected for $(M + H)^+$, 4248.3], respectively. Amino acid compositions and peptide concentrations of stock solutions used in various assays were determined by quantitative amino acid analysis as described previously (*23*).

[1] Abbreviations: Aib or B, 2-aminoisobutyric acid; CD, circular dichroism; DCC, *N*,*N*-dicyclohexylcalbodiimide; DIEA, *N*,*N*-diisopropyl-ethylamine; DMF, *N*,*N*-dimethylformamide; DPhPC, diphytanoylphosphatidylcholine; DPPC, dipalmitoylphosphatidylcholine; DTT, dithiothreitol; Fmoc, 9-fluorenylmethoxycarbonyl; HBTU, 2-(1*H*-benzotriazole-1-yl)-1,1,3,3-tetramethyl-uronium hexafluorophosphate; HEPES, 2-[4-(2-hydroxyethyl)-1-piperazinyl]ethanesulfonic acid; HOBt, 1-hydroxybenzotriazole, MALDI−TOF MS, matrix-assisted laser desorption ionization time-of-flight mass spectrometry; Rink amide resin, 4-(2′,4′-dimethoxyphenyl-Fmoc-aminomethyl)phenoxy resin; RP-HPLC, reversed-phase high-performance liquid chromatography; TFA, 2,2,2-trifluoroacetic acid; TIS, triisopropylsilane.

CD Measurements. CD spectra were recorded on a Jasco J-720 spectropolarimeter (Jasco, Tokyo, Japan) at room temperature. Cylindrical cells with 0.02 or 0.2 cm path lengths were used for measurements. Far-UV CD experiments were carried out in the wavelength range between 190 and 260 nm. Four scans were averaged for each sample, and the blank was subtracted from all spectra. Prepared sample solutions were left at room temperature for 30 min before measurements. The results are expressed as the mean residue ellipticity (θ) with units of degrees cm^2 dmol^{-1}. The helix contents of model peptides were given according to Chen's method (*26*).

Preparation of Small Unilamellar Vesicles (SUVs). DPPC (8.8 μmol) was dissolved in chloroform (100 μL); the chloroform was evaporated by stream of N_2 gas; and the sample was then dried in vacuo overnight. The lipid film was hydrated with 55 mM phosphate buffer (2 mL) and vortexed at 50 °C for 30 min. SUVs were prepared by probe sonication for 20 min using a Branson 250 Sonifier (Branson, Danbury, CT). Calcein-trapped SUVs used for dye-leakage measurements were prepared by a similar method. The lipid film (88 μmol) was hydrated by 2 mL of 100 mM Tris-HCl buffer (pH 7.4) containing 70 mM calcein, and then the suspension was sonicated. Untrapped calcein was removed by gel-filtration chromatography on a Sephadex G-25 column. The lipid concentration was determined by the phosphorus analysis (*27*).

Dye-Leakage Measurements. Dye-leakage measurements were carried out using a Jasco FP-720 spectrofluorophotometer (Jasco) at room temperature. The fluorescence intensity data were collected 40 min after the addition of peptides to SUV-containing buffers. Final lipid concentrations of SUVs were 100 μM. Calcein was excited at 490 nm, and emission at 530 nm was monitored. To determine the fluorescence intensity for 100% dye release, 5 μL of Triton X-100 was added to dissolve and break apart the vesicles. The Triton X-100 treatments were carried out after each measurement. The percentage of dye release caused by the peptides was evaluated by eq 1

$$\text{leakage } \% = [(F_t - F_0)/(F_{100} - F_0)] \times 100 \qquad (1)$$

where F_t is the fluorescence intensity achieved by the peptides and F_0 and F_{100} are fluorescence intensities observed in the absence of the peptides and after Triton X-100 treatment, respectively.

Single-Channel Measurements. Single-channel measurements were performed by the tip-dip technique at room temperature (*21, 28*). Briefly, the patch clamp pipettes were prepared (~1 μm inner diameter) by the two-pulls method using a microelectrode puller (Narishige, Tokyo, Japan) from hematocrit hard grass capillaries (Narishige) without fire polishing. The electrolyte solutions were comprised of 500 mM KCl solutions buffered with 5 mM 2-[4-(2-hydroxyethyl)-1-piperazinyl]ethanesulfonic acid (HEPES) (pH 7.4) or 500 mM KCl and 5 mM HEPES buffer (pH 3.0), which was pH-adjusted by 1 N HCl. Pipettes were filled with the buffer solutions containing peptides. The pipet tip was immersed in a disposable Petri dish filled with the buffer solution. After immersion of the pipet, DPhPC phospholipid monolayer was spread on the surface of the dish solution by careful addition of 1−2 μL of a 10 mg/mL DPhPC solution in hexane. A total of 10 min was allowed for the evaporation of the hexane, and the bilayer was then formed on the pipet tips after reimmersion of pipettes. Seals of 2−20 GΩ were formed at the tip of pipettes. Single-channel currents were amplified using an Axopatch 1D patch-clamp amplifier (Axon Instruments, Inc., Union City, CA) controlled by pClamp 6 software (Axon Instruments, Inc.). Data were filtered at 1 or 2 kHz frequency, stored directly on a hard disk, and analyzed with an AxoGraph 3.5 (Axon Instruments, Inc.). The following cylindrical-bundle model was used to estimate the pore sizes and number of helices involved in the bundle (*29*) (eqs 2 and 3)

$$G = \pi r^2/\rho(l + \pi r/2) \qquad (2)$$

$$r = R[1/\sin(\pi/N) - 1] \qquad (3)$$

where G is the observed conductance, r is the radius of the pore, and N is the number of aggregated helices. The radius of helix (R) is estimated as 0.5 nm; the helix length (l) for the 20-residue peptide is 3.0 nm; and the resistivity (ρ) of 500 mM KCl solution calculated from limiting ionic conductance at 25 °C is 0.13 Ω m (*30*).

Dimeric Model Peptides

K20K20	Ac-Cys-Gly-Gly-(Aib-Lys-Aib-Ala)$_5$-NH$_2$ Ac-Cys-Gly-Gly-(Aib-Lys-Aib-Ala)$_5$-NH$_2$
E20E20	Ac-Cys-Gly-Gly-(Aib-Glu-Aib-Ala)$_5$-NH$_2$ Ac-Cys-Gly-Gly-(Aib-Glu-Aib-Ala)$_5$-NH$_2$
K20E20	Ac-Cys-Gly-Gly-(Aib-Lys-Aib-Ala)$_5$-NH$_2$ Ac-Cys-Gly-Gly-(Aib-Glu-Aib-Ala)$_5$-NH$_2$
anti-K20E20	Ac-Cys-Gly-Gly-(Aib-Lys-Aib-Ala)$_5$-NH$_2$ Ac-(Aib-Glu-Aib-Ala)$_5$-Gly-Gly-Cys-NH$_2$

Monomeric Model Peptides

BKBA20	Ac-(Aib-Lys-Aib-Ala)$_5$-NH$_2$
BEBA20	Ac-(Aib-Glu-Aib-Ala)$_5$-NH$_2$

FIGURE 1: Primary structures of model peptides. K20K20 and E20E20 are homodimers of BKBA20 and BEBA20, respectively. K20E20 and anti-K20E20 are heterodimeric model peptides. The two monomeric helices, BKBA20 and BEBA20, are cross-linked in parallel or antiparallel orientations.

RESULTS

Peptide Design. We have previously reported on syntheses and structural and ion-channel properties of the amphiphilic helical peptide series, Ac-(Aib-Xxx-Aib-Ala)$_5$-NH$_2$ (BXBA20) (*21, 22*). The N and C termini of this sequence were acetylated and amidated, respectively, to cancel termini charges. The unusual amino acid, 2-aminoisobutyric acid (Aib), residues in the peptide sequences are potent inducers of helical structures (*31*). In our previous studies, we have also concluded that at least 20 residues are required for these α-helical peptides to span lipid bilayers (*21*) and reported on helix-forming propensities and ion-channel properties of BKBA20 and BEBA20, containing cationic Lys and anionic Glu residues at the Xxx positions, respectively (*22*). On the basis of these two monomeric parent peptides, we have designed two homo- and two heterodimeric model peptides (Figure 1). Helical peptides were cross-linked via a disulfide bond at termini Cys side chains, and two Gly residues were inserted between the individual helices and Cys residues as spacers (*32*). K20E20 and anti-K20E20 have been designed

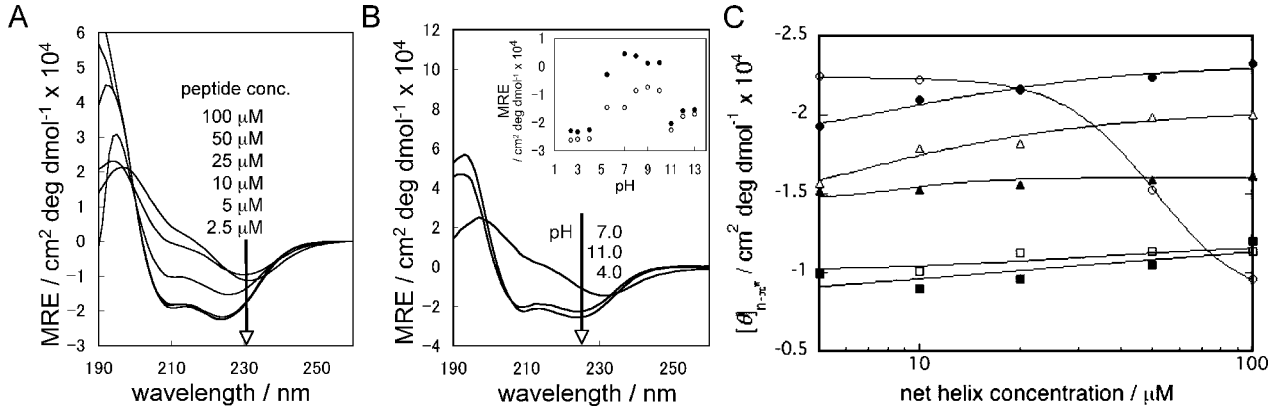

FIGURE 2: CD spectra of model peptides collected in the aqueous solution. All measurements were carried out in 50 mM phosphate buffer. (A) Concentration-dependent spectral changes of K20E20. The spectra were collected at neutral pH conditions (pH 7.4). The α-helical patterns of K20E20 spectra are gradually transformed with the incremental increase in the peptide concentration. (B) pH-dependence of the K20E20 CD spectra. The peptide concentration is 100 μM. A typical α-helical pattern is observed in Glu or Lys side-chain uncharged conditions. (Inset) pH dependence of $[\theta]_{n-\pi^*}$ (○) and $[\theta]_{\pi-\pi^*||}$ (●). Spectra show a drastic change at the pK_a of Lys (pK_a of ϵ-NH_2 = 10.5) and Glu (pK_a of γ-COOH = 4.1) side chains. (C) Concentration dependence of $[\theta]_{n-\pi^*}$ of model peptides. Data were collected at neutral pH conditions (pH 7.4). Symbols represent K20E20 (○), anti-K20E20 (●), K20K20 (△), BKBA20 (▲), E20E20 (□), and BEBA20 (■). $[\theta]_{n-\pi^*}$ in K20E20 decreases at net helix concentrations above 20 μM.

as heterodimeric model peptides. K20E20 and anti-K20E20 are cross-linked analogues with parallel and antiparallel orientations of helices, respectively. The anti-K20E20 was synthesized to estimate the effect of helix orientation for ion-channel activities. K20K20 and E20E20, the respective homodimeric peptides of BKBA20 and BEBA20, were used as reference peptides to estimate the effects of electrostatic interactions.

Model Peptide Structures and Interhelical Interaction. Conformations and molecular interaction of model peptides in aqueous solution were evaluated by CD spectroscopy in 50 mM phosphate buffer (pH 7.4). Generally, CD spectra of all peptides, with the exception of K20E20 at higher concentrations, showed typical α-helical conformations with characteristic double minima around 207 and 224 nm and a maximum around 195 nm. K20E20 also showed typical α-helix structures under lower peptide concentrations, although spectra gradually changed to the patterns with single minima around 231 nm and single maxima around 197 nm as an increase of the peptide concentration (Figure 2A). It seems that the spectral change reflected intermolecular association of K20E20 because the changes were concentration-dependent. The anti-K20E20 did not show this spectral change. Typical patterns of the α-helix were conserved at all examined peptide concentrations. Thereby, it seems that the concentration-dependent changes in CD spectra of these two peptides were influenced by the helix orientation. Figure 2B shows the pH titration CD spectra of K20E20 at 100 μM peptide concentration. The pK_a of ϵ-amino groups of Lys is 10.5, and the pK_a of γ-carboxyl groups of Glu is 4.1. The CD spectrum of associated K20E20 (at 100 μM) was converted to a typical α-helix spectrum at low pH (uncharged Glu; pH ≤ 4.0) or high pH (uncharged Lys; pH ≥ 11) conditions. These results suggest that the interhelical electrostatic interaction between side chains strongly affects the intermolecular association of K20E20 at high peptide concentrations. At low peptide concentrations, the electrostatic interaction is possibly limited to intramolecular ion-pair formation or disruption (low or high pH) of K20E20. The negative band around 224 nm derived from the n−π* transition ($[\theta]_{n-\pi^*}$) correlates to the helical content of the overall secondary structure (*26*). Figure 2C shows the relationship of the concentration and helical content (ellipticity at $[\theta]_{n-\pi^*}$) of model peptides. With the exception of K20E20, the ellipticities of all model peptides did not show significant concentration dependence. According to the concentration dependent CD measurements, the intermolecular association of K20E20 was negligible at concentrations lower than 10 μM (net helix concentration of 20 μM). Subsequent CD measurements were carried out at this concentration to avoid the intermolecular association of K20E20. In the absence of the intermolecular interactions leading to peptide association, at the 20 μM net helix concentration, helix contents of K20E20, anti-K20E20, K20K20, E20E20, BKBA20, and BEBA20 were 64, 64, 52, 29, 44, and 24%, respectively. Helix contents of cationic peptides are larger than those of anionic peptides, and homodimeric peptides showed larger helix contents than their respective monomers. Heterodimeric model peptides exhibited highest helix contents among model peptides. These results suggested that the helical conformations in heterodimeric peptides were stabilized by intramolecular electrostatic interactions.

To assess helix−helix interactions between cationic and anionic monomeric peptides, mixing ratios of BKBA20 and BEBA20 were gradually changed and CD spectra were measured to monitor the conformational change (Figure 3). The relationship of the $[\theta]_{n-\pi^*}$ versus the monomeric peptide mixing ratios was linear, and therefore, no measurable interhelical interactions between the monomeric peptides were detected. Mixing of K20K20 and E20E20 also did not show any increase in overall helical contents, implying the absence of the intermolecular interaction between the dimeric peptides. The $[\theta]_{n-\pi^*}$ ellipticities in the CD spectra of K20E20 and anti-K20E20 were decreased to comparable levels to those of monomeric peptides after cleavage of disulfide linkage with 1 mM dithiothreitol (DTT) treatments. These results further confirmed that electrostatic interactions existed in heterodimeric peptides and covalent dimerization of helices was a requisite for this interaction.

Peptide−Membrane Interactions and Structural Change in Lipid Bilayers. To explore the structural changes of model

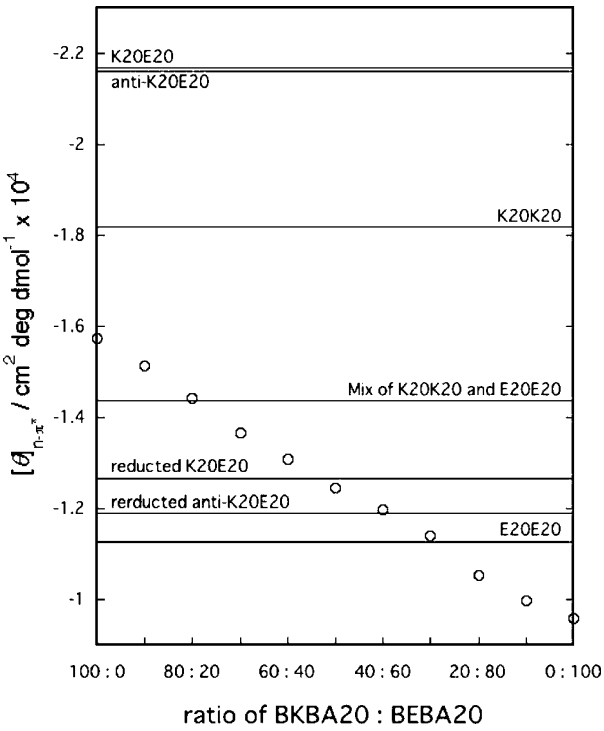

FIGURE 3: Mean residue ellipticities at n$-\pi^*$ transitions ($[\theta]_{n-\pi^*}$) of model peptides. The spectra were corrected in 50 mM phosphate buffers (pH 7.4). Net helix concentrations are 20 μM. (○) $[\theta]_{n-\pi^*}$ at variable mixing ratios of BKBA20 and BEBA20. The transition of $[\theta]_{n-\pi^*}$ is linear: no interactions are observed between the monomeric helices. Mixing of K20K20 and E20E20 also does not show an increase in $[\theta]_{n-\pi^*}$. The helical contents and helix$-$helix interactions of heterodimeric peptides were decreased by a reduction of the disulfide linkage with 1 mM DTT treatments.

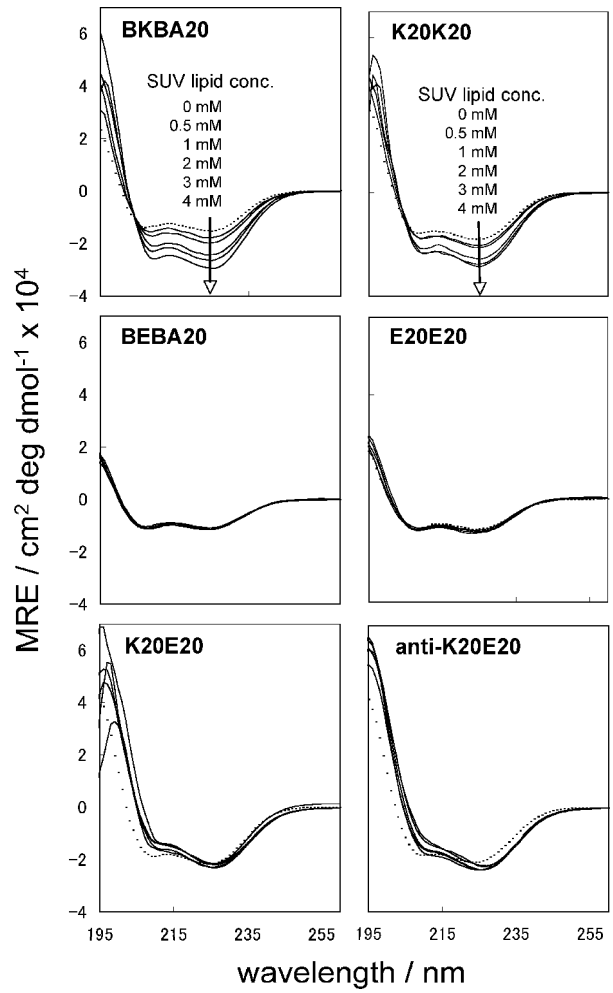

FIGURE 4: Liposome-concentration-dependent CD measurements. Net helix concentrations are 20 μM. The spectra were collected at neutral pH conditions (pH 7.4). Dotted and solid lines represent spectra recorded in the absence or presence of DPPC SUVs, respectively. Concentrations of DPPC are 0.5, 1, 2, 3, and 4 mM. Cationic peptides (upper) exhibit successive spectral changes corresponding to the lipid concentration. Anionic peptides (middle) do not show any spectral change in all conditions. Spectra of heterodimeric peptides (lower) show a significant increase of the $[\theta]_{n-\pi^*}/[\theta]_{\pi-\pi^*||}$ ratios and red shifts of the $\pi-\pi^*||$ band in the presence of DPPC SUVs. These spectral changes did not depend upon the measured lipid concentrations.

peptides in phospholipid bilayers and assess the membrane affinities of these peptides, titration CD spectra were measured in DPPC lipid vesicles (Figure 4). A red shift of the $\pi-\pi^*||$ transition band (the minimum around 207 nm), and an increase in the $[\theta]_{n-\pi^*}/[\theta]_{\pi-\pi^*||}$ ratio suggest two-stranded helix association (*14, 33*). It is worth mentioning that the $[\theta]_{n-\pi^*}/[\theta]_{\pi-\pi^*||}$ ratios of the two heterodimeric peptides were significantly increased in the presence of DPPC SUVs. The ratios of K20E20 and anti-K20E20 in 50 mM phosphate buffers were both 1.15, and these ratios were increased to 1.56 and 1.84, respectively, in the presence of 4 mM DPPC SUVs. In addition, minimum ellipticity of the $\pi-\pi^*||$ transitions in heterodimer peptides shifted to 211–212 nm in the presence of DPPC SUVs. Other peptides did not exhibit significant changes either in their ellipticity ratios or $\pi-\pi^*||$ minimum ellipticities. These results strongly suggested the two-stranded helix association of the heterodimeric peptides in phospholipid bilayers. Moreover, the spectral change did not depend upon lipid concentrations. Indistinguishable spectra were obtained at all measured lipid concentrations, implying high membrane affinities of heterodimeric peptides for phospholipid bilayers (*34*). CD spectra of BKBA20 and K20K20 were increased in a lipid-concentration-dependent manner. Isodichroic points found around 205 nm in the spectra of these peptides indicated an equilibrium between membrane-bound and free cationic peptides. Relative affinities and helix association propensities of cationic peptides were less than those of heterodimeric peptides. BEBA20 and E20E20 did not show any spectral change by the addition of SUVs; thus, no peptide$-$lipid interactions were detected.

Membrane Perturbation Activities of Model Peptides. Dye-leakage measurements were carried out to assess membrane perturbation activities of model peptides against zwitterionic DPPC membranes (Figure 5). BKBA20 and K20K20 exhibited distinct membrane perturbation (~50 and ~30%, respectively) at 2 μM net helix concentrations. K20E20 and anti-K20E20 showed higher leakage activity than those of cationic peptides; both peptides showed over 90% activities at comparable concentrations. None or negligible membrane perturbation activities were observed for the anionic peptides.

Channel-Forming Properties of Model Peptides. Ion-channel activities of the model peptides were evaluated by the tip-dip technique on zwitterionic and mechanically stable DPhPC bilayers. Because of the small dimensions of bilayers, the technique permits low noise levels (*28*). Channel conductance (G) is expressed as the reciprocal resistance with units of siemens (S). In our previous studies, BKBA20 at

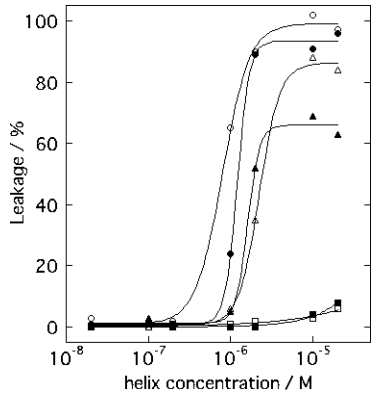

FIGURE 5: Concentration-dependent dye-leakage measurements. DPPC concentrations of calcein-trapped SUVs are 100 μM in all measurements. Symbols represent K20E20 (○), anti-K20E20 (●), K20K20 (△), BKBA20 (▲), E20E20 (□), and BEBA20 (■). Heterodimeric peptides exhibit higher leakage activities compared to those of cationic peptides.

100 nM peptide concentration showed single-level ion conductance of 228 pS (*21*). According to the cylindrical bundle model (*29*), the pore was composed of tetramerical helices with 0.35 nm pore diameter. BEBA20 showed multilevel conductance patterns with large conductance values (*22*). Typical conductance patterns of homodimeric model peptides were illustrated in Figure 6A. K20K20 exhibited single-state conductance patterns including spiky current fluctuation at 50 nM peptide concentration. The single-level conductance pattern with ca. 230 pS conductivity was observed occasionally at 5 nM peptide concentration (net helix concentration of 10 nM). In comparison, ion channels of K20K20 were detected at lower peptide concentrations than those of BKBA20 (*21*), implying favorable entropic factors resulted from covalent dimerization in the former peptide. Similarly, the conductance patterns of E20E20 at 50 nM were also different from those of BEBA20. However, small and single-state conductance patterns were only occasionally observed in E20E20. A clear interpretation of the differences of conductance patterns between di- and monomeric anionic peptides could not be obtained from our observations.

Concentration dependence of ion-channel activities of K20E20 is illustrated in Figure 6B. The erratic conductance patterns were detected in the 10–100 nM peptide concentration range with high frequencies. As the peptide concentration decreased, the current fluctuations also decreased. Finally, at 1 nM concentration, the ion-channel activity of K20E20 was well-resolved with distinct open−close states. Figure 6C exhibits conductance patterns of 1 nM K20E20 recorded under various membrane potentials. This measurement was reproducible under similar conditions, and the conductance patterns showed voltage dependence of mean channel-opening durations. Individual channel-opening durations of K20E20 (at 1 nM) were at millisecond order time scales. The channel lifetime was comparable to those of other model peptides recorded at higher peptide concentrations. An ohmic linear I−V relationship for the open state of the main channel of K20E20 is exhibited in Figure 6D. The ion conductance in this stable channel is constant and equal to the slope of the line. The mean conductivity of K20E20 was approximately 1.5 nS under all membrane potentials. The calculated pore diameter was ca. 1.0 nm, which corresponded to a hexameric helix bundle. Overall, K20E20 showed distinct ion-channel activities, whereas anti-K20E20 did not exhibit ion channels with well-resolved open−close states under comparable conditions (data not shown).

Effects of pH on the Structure and Ion-Channel Activities of K20E20. If the formation of K20E20 ion channels was assisted by the existence of interhelical ion pairs, structural disorder and perturbation of channel activity should occur by any disruption in the ion-pair network. To investigate the validity of this assumption, liposome titration CD spectra of K20E20 were measured in acidic media (pH 3.0) to assess whether the neutralization of the negative charge of Glu side chains affected the high degree of helix association and the high membrane affinity of K20E20 (Figure 7). No significant difference in the $[\theta]_{n-\pi^*}/[\theta]_{\pi-\pi^*||}$ ratio and the red shift of the $\pi-\pi^*||$ band was detected in the absence or presence of DPPC vesicles. However, spectra were dependent upon the lipid concentration, and an isodichroic point appeared at ~205 nm. These results indicated that the helix association propensities as well as the membrane affinities of K20E20 were diminished by a decrease and disruption in the electrostatic interhelical interactions at low pH. Same experiments were carried out for monomeric peptides. Both BKBA20 and BEBA20 showed lipid-concentration-dependent spectral changes. It is notable that the membrane interaction of BEBA20 in neutral pH conditions was also altered under acidic conditions.

Ion-channel activities of K20E20 were also measured under acidic conditions at pH 3.0 (Figure 8A). Conductance patterns of 50 nM K20E20 recorded in neutral pH exhibited erratic conductance patterns, while the conductance patterns were converted to single states with clear open−close transition under acidic conditions. Relative ion conductivities at neutral pH were quite large, but in comparison, the ion coductivity under acidic conditions was considerably smaller. Under acidic conditions, the mean conductivity was 174 pS, which corresponded to tri- or tetramerical helix bundles.

DISCUSSION

Effects of Electrostatically Assisted Helix Association on Membrane Interaction and Formation of Ion Channels. Generally, two-stranded coils of ion-channel helices have been presumed as an intermediate in the helix-bundle-assembling process (*2, 8, 10, 11*). In the present study, ion-channel formation was detected in covalently connected hybrid cationic and anionic interacting helices. It is expected that in these heterodimeric peptides the tight helix−helix interaction, supported by interhelical salt bridges, could directly promote the formation of helical bundle assemblies in phospholipid bilayers by bypassing the formation of double-stranded associated intermediates. An increase in the helical contents of these chimeric peptides, in comparison to monomeric or homodimeric peptides, was a strong indication of the contribution of electrostatic interactions in the helix−helix interaction and stabilization. However, the contribution of intramolecular hydrophobic interactions in the stabilization of heterodimeric peptides could not be easily evaluated in the presence of electrostatic interactions.

As a result of ionic and/or polar interactions between the hydrophilic surfaces of amphiphilic heterodimeric peptides, the hydrophobic surfaces of these peptides are externalized

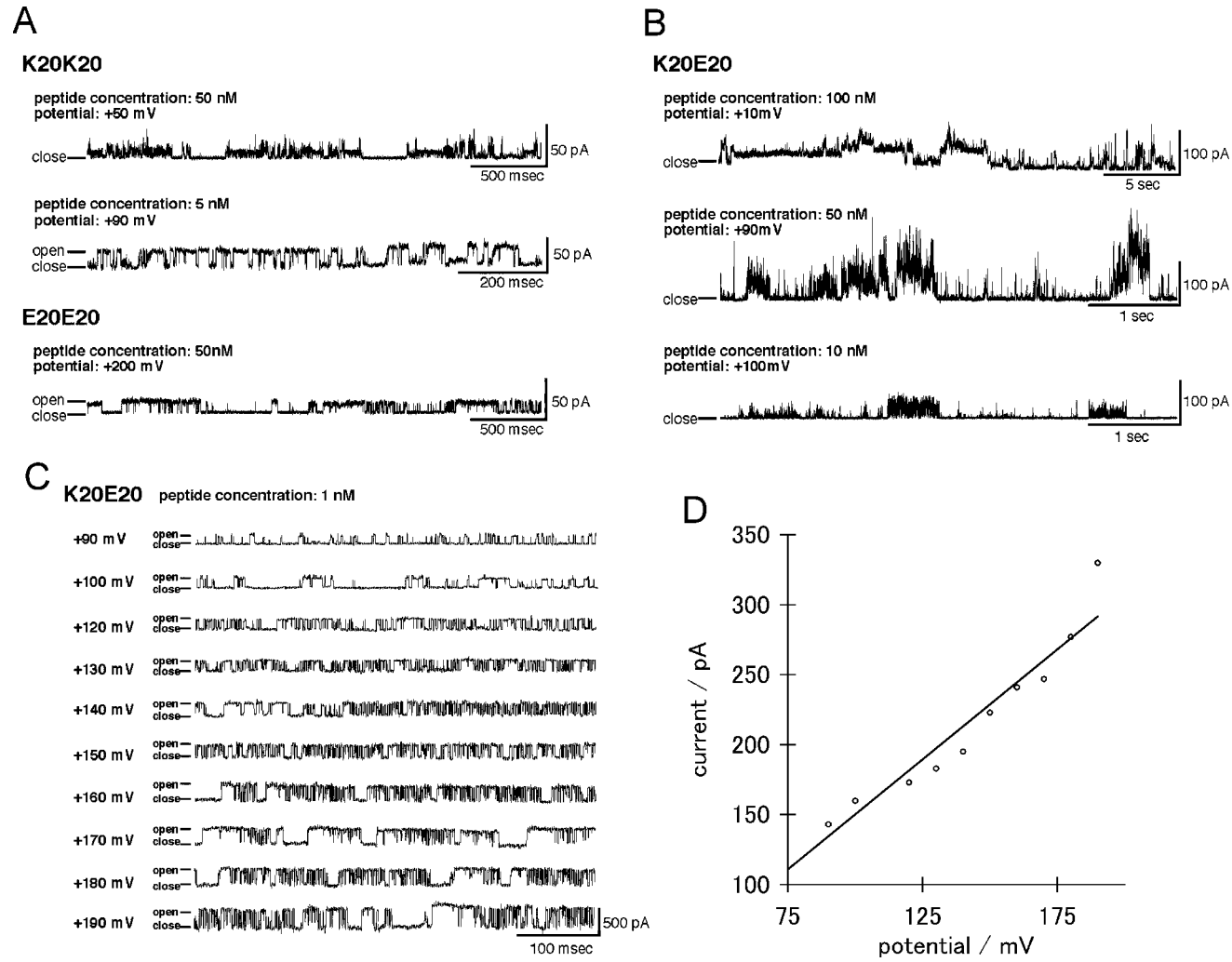

FIGURE 6: Representative single-channel conductance patterns of the dimeric model peptides. Measurements were carried out under neutral (pH 7.4) conditions. (A) Conductance patterns of homodimeric model peptides. K20K20 occasionally exhibited clear open−close transitions of the ion channel at 5 nM peptide concentrations. (B) Conductance patterns of K20E20 under 10–100 nM peptide concentrations. Erratic patterns were dominantly observed at this peptide concentration range. (C) Ion-channel properties of K20E20 at 1 nM peptide concentrations. Conductance patterns recorded under variable membrane potentials (from +90 to +190 mV). (D) I−V plot for 1 nM K20E20 at variable membrane potentials. A linear I−V relationship is observed.

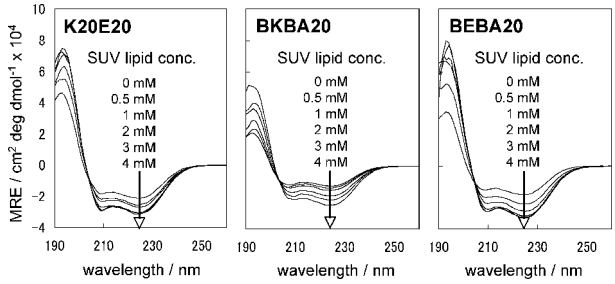

FIGURE 7: Liposome-concentration-dependent CD spectra recorded under acidic conditions. Measurements were carried out in 50 mM phosphate buffers (pH 3.0), in the presence and absence of DPPC SUVs. Net helix concentrations are 20 μM. Spectral changes of all model peptides are lipid-concentration-dependent. Isodichroic points are found at 205 nm in each spectrum. Significant differences of the $[\theta]_{n\text{-}\pi^*}/[\theta]_{\pi\text{-}\pi^*||}$ ratios and π−π^*|| band in the absence or presence of DPPC SUVs were not observed.

and exposed. Hydrophobicity has been widely accepted as an important factor for the interaction of peptides and proteins with zwitterionic phospholipid bilayers (*35*). Significant dye-leakage activities and high membrane affinities of heterodimeric peptides against DPPC membranes also imply higher peptide hydrophobicity; rather than remaining in aqueous environments, the heterodimeric peptides prefer to accumulate on membrane surfaces and partition into them. This high membrane affinity of the heterodimeric peptides should therefore allow for the penetration and association of these peptides in membrane interiors, leading to the formation of appropriate homomeric ion-conducting channels even at considerably low peptide concentrations (as low as 1 nM).

Popot and Engelman proposed a two-stage folding model of α-helical membrane proteins (*36, 37*). The first step involves independent insertion of individual helices into the membrane, and in the second step, the inserted transmembrane helices interact and associate. On the basis of this model, both high membrane affinity and self-association properties of the heterodimeric peptides facilitate helix-bundle formation in lipid bilayers. In fact, K20E20 had a clear open−close transition of its ion channel even under extremely low peptide concentrations. The design of amphiphilic helical constructs with hydrophilic oppositely charged surfaces therefore seems to be an appropriate method to promote and facilitate the formation of helical-bundle assemblies in lipid membranes. The two heterodimeric

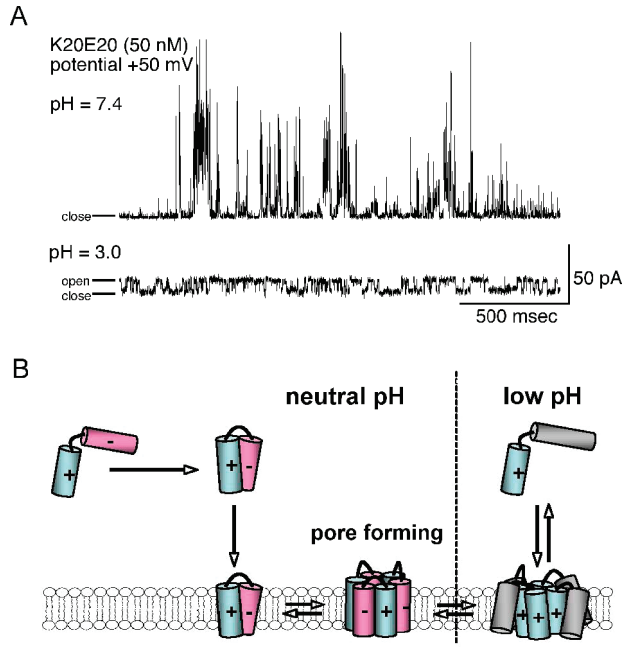

FIGURE 8: pH effects on ion-channel activities of K20E20. (A) Comparison of K20E20 conductance patterns recorded under neutral (pH 7.4) and acidic (pH 3.0) conditions. The dimeric peptide concentration in both conditions is 50 nM. The applied potential is +50 mV in both traces. Erratic conductance patterns with large ion conductivity were recorded in the neutral pH conditions, and the patterns were converted to single-state conductance patterns in the acidic conditions. (B) Suggested scheme for the pore-forming mechanism and pH-sensitive behavior of K20E20. Equilibriums of two-stranded helix association and peptide membrane interactions are favored by interhelical electrostatic interactions, and ion-channel formation is facilitated. The channel-forming ability is degraded in the acidic conditions because of the disordered electrostatic interactions. Note that the pore forming in acidic conditions may require higher peptide concentrations than neutral conditions.

peptides, K20E20 and anti-K20E20, possess comparable membrane affinities and helix association propensities; however, anti-K20E20 did not exhibit well-resolved ion-channel activities. In the presence of a transmembrane potential, macrodipole moments of helical structures interact with the external electric field and as a result of this interaction are oriented perpendicular to the membrane surface (*38*). In the case of anti-K20E20, it seems that, as a result of the antiparallel orientation of the macrodipoles of its helical components, stable ion-conducting assemblies could not be formed for this peptide in lipid membranes. The parallel orientation of helices is therefore a necessary requirement for the ion channels formed of helical bundles.

In accordance with the barrel-stave model (*6*), the pore size is dependent upon the number of incorporated helices in the bundle. Consequently, an increase or a decrease in the number of helices results in various conductance levels. Therefore, helix bundles consisting of a specific number of helices have a good potential to be employed as scaffolds for various functional modifications of the pores. Thus far, many efforts have been directed to control helix association: especially, chemical cross-linking techniques have been used to regulate pore structures. The technique of template-assembled synthetic protein (TASP), proposed by Mutter, has been employed to control helix numbers and orientations, as well as the helix components in a bundle structure (*39*). Several investigations have previously reported on the construction of controlled pore sizes using this approach (*40*). Single-state conductance of 1 nM K20E20 is a specific case for the stabilization of the helix bundle with hexameric helices. No subconductance levels were observed in this simple ion channel, which was selectively stabilized without possessing an elaborate molecular design. A common feature of the mechanism of cation/anion selectivity is that the chemical nature and structure of the amino acid side chains located in proximity of the pore region can act as selective filters by selecting ions based on their polarity and charge density (*41, 42*). We have already reported the mild cation selectivity of BEBA20 and the nonspecific ion selectivity of BKBA20 (*22*); however, the cation/anion selectivity concepts could not be easily applied in the case of K20E20, because an equal number of cationic and anionic amino acid side chains coexist in this peptide.

The mean opening duration of K20E20 ion channels was voltage-dependent; however, the duration of individual channel openings was not significantly elongated. One possible interpretation for this observation is that the dimer–dimer intermolecular interactions were not or only weakly enhanced by ion-pair formation between heterodimeric helices in the bundle structure. You et al. and Okazaki et al. reported that the channel lifetimes of alamethicin were drastically increased by helix dimerization (*43, 44*). The glutamine at position 7 of alamethicin lining the interior of the channel is assumed to stabilize the helix bundles by hydrogen-bonding networks that could promote helix−helix interactions in the ion-channel helical bundle (*45*). To obtain longer pore-opening durations, further stabilization of pores with an emphasis on dimer–dimer interactions in the bundle will be examined in our future studies.

Modulation of Ion-Channel Activity by Electrostatic Interactions. The ion-channel forming of K20E20 facilitated by the interhelical electrostatic interaction of ionic pairs suggests the possibility of modulation of ion-channel characteristics by modifying the pH. Several reports have mentioned that the pH alteration caused conformational disorder or unfolding of helices stabilized by intra- or interhelical salt bridges (*46, 47*). Thus, the assembly of helical bundles assisted by salt bridges should be destabilized by a decrease in electrostatic interactions, resulting in possible ion-channel inactivation. Modulation of the helical bundle formation by modification of pH or ionic strength can therefore be used as a general method to control the activation or inactivation of the engineered synthetic ion-channel peptides. According to the DPPC vesicle titration CD measurements, performed under low pH conditions, the membrane affinity as well as helix association propensity of K20E20 in phospholipid bilayers were reduced in comparison to the neutral pH conditions. Moreover, the erratic but large conductivity of K20E20 channels under neutral pH conditions was switched to a single-level low conductivity state under acidic conditions. Figure 8B exhibits a schematic drawing of the bundle-forming process by K20E20 under neutral and low pH conditions. As shown in this scheme, the ion pairs in K20E20 provide the intermediates of helix bundles under neutral pH conditions; however, under acidic conditions, the ion pairs cease to interact because of the protonation of Glu side chains. Interestingly, the ion conductance patterns and conductivities of K20E20 recorded in the acidic medium are similar to those of BKBA20 (*21–23*); therefore, it seems

plausible that the ion conductance activity is caused by channels composed of only the BKBA20 domains of the heterodimeric peptides. The BEBA20 domain should not be capable of forming ion channels under acidic conditions because of the considerable reduction of helix amphiphilicity. Nevertheless, the membrane interaction of BEBA20 observed under acidic conditions can not be completely ignored. Some helical peptides containing neutralized carboxyl groups can interact with lipid membranes under acidic conditions (*48, 49*). Whether the BEBA20 segments are involved in the ion-conducting structures of K20E20 pores can not be verified at the present stage.

Electrostatic interactions play a critical role not only in stabilizing the helix segments in the intact proteins but also in the process of membrane incorporation. It has been reported that the S4 helical segment of the Shaker and related ion-channel proteins, possessing many cationic residues, are inserted into biological membranes after forming ion pairs with anionic helical domains (*50*). In addition, electrostatic interactions play important roles in the biological functions of ion-channel proteins (*51*). In a recent study, the pH-sensing domain of acid-sensing ion-channel (ASIC) protein was identified at a far distance from the pore region and an electrostatic carboxyl−carboxylate interaction acted as a trigger for ion-channel activation/deactivation (*52*). Our designed synthetic peptides, K20E20, also formed pH-sensitive ion channels in phospholipid bilayers and responded to the changes in pH by modifying its conductance patterns. Because the conductance in K20E20 ion channels could be modulated by changes in pH, this peptide can serve as a minimalist model for pH-sensing ion-channel proteins.

ACKNOWLEDGMENT

We are grateful to Professor Yasuyuki Shimohigahsi (Kyushu University) and Dr. Hideki Ohba (National Institute of Advanced Industrial Science and Technology, Japan) for the use of MALDI−TOF MS.

REFERENCES

1. Spach, G., Duclohier, H., Molle, G., and Valleton, J. M. (1989) Structure and supramolecular architecture of membrane channel forming peptides. *Biochimie 71*, 11–21.
2. Lear, J. D., Wasserman, Z. R., and DeGrado, W. F. (1988) Synthetic amphiphilic peptide models for protein ion channels. *Science 240*, 1177–1181.
3. Woolley, G. A., and Wallace, B. A. (1992) Model ion channels: Gramicidin and alamethicin. *J. Membr. Biol. 129*, 109–136.
4. Iwata, T., Lee, S., Oishi, O., Aoyagi, H., Ohno, M., Anzai, K., Kirino, Y., and Sugihara, G. (1994) Design and synthesis of amphipathic 3_{10}-helical peptides and their interactions with phospholipid bilayers and ion channel formation. *J. Biol. Chem. 269*, 4928–4933.
5. Ghadiri, M. R., Granja, J. R., and Buehler, L. K. (1994) Artificial transmembrane ion channels from self-assembling peptide nanotubes. *Nature 369*, 301–304.
6. Baumann, G., and Mueller, P. (1974) A molecular model of membrane excitability. *J. Supramol. Struct. 2*, 538–557.
7. Montal, M. (1990) Molecular anatomy and molecular design of channel proteins. *FASEB J. 4*, 2623–2635.
8. DeGrado, W. F., Wasserman, Z. R., and Lear, J. D. (1989) Protein design, a minimalist approach. *Science 243*, 622–628.
9. DeGrado, W. F., Summa, C. M., Pavone, V., Nastri, F., and Lombardi, A. (1999) De novo design and structural characterization of proteins and metalloproteins. *Annu. Rev. Biochem. 68*, 779–819.
10. Chung, L. A., Lear, J. D., and DeGrado, W. F. (1992) Fluorescence studies of the secondary structure and orientation of a model ion channel peptide in phospholipid vesicles. *Biochemistry 31*, 6608–6616.
11. Woolley, G. A., and Wallace, B. A. (1993) Temperature dependence of the interaction of alamethicin helices in membranes. *Biochemistry 32*, 9819–9825.
12. Hodges, R. S., Saund, A. K., Chong, P. C. S., St.-Pierre, S. A., and Reid, R. E. (1981) Synthetic model for two-stranded α-helical coiled-coils: Design, synthesis, and characterization of an 86-residue analog of tropomyosin. *J. Biol. Chem. 256*, 1214–1224.
13. Lau, S. Y. M., Taneja, A. K., and Hodges, R. S. (1984) Synthesis of a model protein of defined secondary and quaternary structure: Effect of chain length on the stabilization and formation of two-stranded α-helical coiled-coils. *J. Biol. Chem. 259*, 13253–13261.
14. Zhou, N. E., Kay, C. M., and Hodges, R. S. (1992) Synthetic model proteins: Positional effects of interchain hydrophobic interactions on stability of two-stranded α-helical coiled-coils. *J. Biol. Chem. 267*, 2664–2670.
15. Zhou, N. E., Kay, C. M., and Hodges, R. S. (1994) The role of interhelical ionic interactions in controlling protein folding and stability: De novo designed synthetic two-stranded α-helical coiled-coils. *J. Mol. Biol. 237*, 500–512.
16. Gratkowski, H., Lear, J. D., and DeGrado, W. F. (2001) Polar side chains drive the association of model transmembrane peptides. *Proc. Natl. Acad. Sci. U.S.A. 98*, 880–885.
17. Dawson, J. P., Melnyk, R. A., Deber, C. M., and Engelman, D. M. (2003) Sequence context strongly modulates association of polar residues in transmembrane helices. *J. Mol. Biol. 331*, 255–262.
18. Zhou, F. X., Merianos, H. J., Brunger, A. T., and Engelman, D. M. (2001) Polar residues drive association of polyleucine transmembrane helices. *Proc. Natl. Acad. Sci. U.S.A. 98*, 2250–2255.
19. Johnson, R. M., Heslop, C. L., and Deber, C. M. (2004) Hydrophobic helical hairpins: Design and packing interactions in membrane environments. *Biochemistry 43*, 14361–14369.
20. Johnson, R. M., Hecht, K., and Deber, C. M. (2007) Aromatic and cation−π interactions enhance helix−helix association in a membrane environment. *Biochemistry 46*, 9208–9214.
21. Higashimoto, Y., Kodama, H., Jelokhani-Niaraki, M., Kato, F., and Kondo, M. (1999) Structure−function relationship of model Aib-containing peptides as ion transfer intermembrane templates. *J. Biochem. 125*, 705–712.
22. Hara, T., Kodama, H., Higashimoto, Y., Yamaguchi, H., Jelokhani-Niaraki, M., Ehara, T., and Kondo, M. (2001) Side chain effect on ion channel characters of Aib rich peptides. *J. Biochem. 130*, 749–755.
23. Yamaguchi, H., Kodama, H., Osada, S., Jelokhani-Niaraki, M., Kato, F., and Kondo, M. (2002) The position of Aib residues defines the antimicrobial activity of Aib-containing peptides. *Bull. Chem. Soc. Jpn. 75*, 1563–1568.
24. Kiwada, T., Sonomura, K., Sugiura, Y., Asami, K., and Futaki, S. (2006) Transmission of extramembrane conformational change into current: Construction of metal-gated ion channel. *J. Am. Chem. Soc. 128*, 6010–6011.
25. Zhang, Y., Futaki, S., Kiwada, T., and Sugiura, Y. (2002) Detection of protein−ligand interaction on the membranes using C-terminus biotin-tagged alamethicin. *Bioorg. Med. Chem. 10*, 2635–2639.
26. Chen, Y. H., Yang, J. T., and Martinez, H. M. (1972) Determination of the secondary structures of proteins by circular dichroism and optical rotatory dispersion. *Biochemistry 11*, 4120–4131.
27. Bartlett, G. R. (1959) Phosphorus assay in column chromatography. *J. Biol. Chem. 234*, 466–468.
28. Coronado, R., and Latorre, R. (1983) Phospholipid bilayers made from monolayers on patch-clamp pipettes. *Biophys. J. 43*, 231–236.
29. Sansom, M. S. P. (1993) Alamethicin and related peptaibols-model ion channels. *Eur. Biophys. J. 22*, 105–124.
30. Robinson, R. A., and Stokes, R. H. (1970) *Electrolyte Solutions*, 2nd ed., Butterworths, London, U.K.
31. Burgess, A. W., and Leach, S. J. (1973) An obligatory α-helical amino acid residue. *Biopolymers 12*, 2599–2605.
32. Talanian, R. V., McKnight, C. J., and Kim, P. S. (1990) Sequence-specific DNA binding by a short peptide dimer. *Science 249*, 769–771.
33. Cooper, T. M., and Woody, R. W. (1990) The effect of conformation on the CD of interacting helices: A theoretical study of tropomyosin. *Biopolymers 30*, 657–676.

34. White, S. H., Wimley, W. C., Ladokhin, A. S., and Hristova, K. (1998) Protein folding in membranes: Determining energetics of peptide−bilayer interactions. *Methods Enzymol. 295*, 62–87.
35. Matsuzaki, K. (1999) Why and how are peptide−lipid interactions utilized for self-defence? Magainins and tachyplesins as archetypes. *Biochim. Biophys. Acta 1373*, 137–146.
36. Popot, J. L., and Engelman, D. M. (1990) Membrane protein folding and oligomerization: The two-stage model. *Biochemistry 29*, 4031–4037.
37. Engelman, D. M., Chen, Y., Chin, C. N., Curran, A. R., Dixon, A. M., Dupuy, A. D., Lee, A. S., Lehnert, U., Matthews, E. E., Reshetnyak, Y. K., Senes, A., and Popot, J. L. (2003) Membrane protein folding: Beyond the two stage model. *FEBS Lett. 555*, 122–125.
38. Sansom, M. S. P. (1991) The biophysics of peptide models of ion channels. *Prog. Biophys. Mol. Biol. 55*, 139–235.
39. Mutter, M., and Vuilleumier, S. (1989) A chemical approach to protein design-template-assembled synthetic proteins (TASP). *Angew. Chem., Int. Ed. Engl. 28*, 535–554.
40. Matsubara, A., Asami, K., Akagi, A., and Nishino, N. (1996) Ion-channels of cyclic template-assembled alamethicins that emulate the pore structure predicted by the barrel-stave model. *Chem. Commun.* 2069–2070.
41. Imoto, K. (1993) Ion channels: Molecular basis of ion selectivity. *FEBS Lett. 325*, 100–103.
42. Starostin, A. V., Butan, R., Borisenko, V., James, D. A., Wenschuh, H., Sansom, M. S. P., and Woolley, G. A. (1999) An anion-selective analogue of the channel-forming peptide alamethicin. *Biochemistry 38*, 6144–6150.
43. You, S., Peng, S., Lien, L., Breed, J., Sansom, M. S. P., and Woolley, G. A. (1996) Engineering stabilized ion channels: Covalent dimers of alamethicin. *Biochemistry 35*, 6225–6232.
44. Okazaki, T., Sakoh, M., Nagaoka, Y., and Asami, K. (2003) Ion channels of alamethicin dimer N-terminally linked by disulfide bond. *Biophys. J. 85*, 267–273.
45. Kaduk, C., Dathe, M., and Bienert, M. (1998) Functional modifications of alamethicin ion channels by substitution of glutamine 7, glycine 11 and proline 14. *Biochim. Biophys. Acta 1373*, 137–146.
46. Marqusee, S., and Baldwin, R. L. (1987) Helix stabilization by $Glu^{-}\cdots Lys^{+}$ salt bridges in short peptides of de novo design. *Proc. Natl. Acad. Sci. U.S.A. 84*, 8898–8902.
47. Dolphin, G. T., and Baltzer, L. (1997) The pH-dependent tertiary structure of a designed helix−loop−helix dimer. *Folding Des. 2*, 319–330.
48. Hunt, J. F., Rath, P., Rothschild, K. J., and Engelman, D. M. (1997) Spontaneous, pH-dependent membrane insertion of a transbilayer α-helix. *Biochemistry 36*, 15177–15192.
49. Davidson, V. L., Brunden, K. R., and Cramer, W. A. (1985) Acidic pH requirement for insertion of colicin E1 into artificial membrane vesicles: Relevance to the mechanism of action of colicins and certain toxins. *Proc. Natl. Acad. Sci. U.S.A. 82*, 1386–1390.
50. Zhang, L., Sato, Y., Hessa, T., Heijne, G., Lee, J. K., Kodama, I., Sakaguchi, M., and Uozumi, N. (2007) Contribution of hydrophobic and electrostatic interactions to the membrane integration of the Shaker K^{+} channel voltage sensor domain. *Proc. Natl. Acad. Sci. U.S.A. 104*, 8263–8268.
51. Bezanilla, F. (2000) The voltage sensor in voltage-dependent ion channels. *Physiol. Rev. 80*, 555–592.
52. Jasti, J., Furukawa, H., Gonzales, E. B., and Gouaux, E. (2007) Structure of acid-sensing ion channel 1 at 1.9 Å resolution and low pH. *Nature 449*, 316–323.

BI702371E